RSC Advances

PAPER

View Article Online
View Journal | View Issue

Cite this: *RSC Adv.*, 2022, **12**, 1628

Microwave-assisted *in situ* ring-opening polymerization of ε-caprolactone in the presence of modified halloysite nanotubes loaded with stannous chloride†

Gang Yang, Rui Ma,* Shifan Zhang, Ziying Liu, Dexuan Pei, Hongyun Jin,* Jiaqi Liu and Wenjie Du

Polycaprolactone (PCL) has been widely applied for its excellent physicochemical properties, but it also has common problems with biopolymers. It is important to investigate energy-efficient polymerization crafts and composite catalytic systems in the ring-opening polymerization (ROP) of ε-caprolactone (ε-CL) to prepare high-performance PCL matrix composites. In this study, a composite catalytic system of modified halloysite nanotubes loaded with stannous chloride (APTES-P-h-HNTs-$SnCl_2$) was successfully synthesized *via* hydroxylation, calcination, silane coupling agent modification and physical loading. It was used to catalyze the microwave-assisted *in situ* ROP of ε-CL to synthesize PCL matrix nanocomposites with modified halloysite nanotubes (PCL-HNTs). The structure, morphology, polymerization, thermal properties and electrochemical performance of products were subsequently investigated. The results show that PCL-HNTs have been successfully synthesized with connected petal-like and porous structures. Compared with PCL, the film-forming and thermal properties of PCL-HNTs have been significantly improved. Moreover, PCL-HNTs have a potential application value in the field of solid polymer electrolytes (SPEs).

Received 8th October 2021
Accepted 8th December 2021

DOI: 10.1039/d1ra07469e

rsc.li/rsc-advances

1. Introduction

As one of the most important biodegradable polymer materials, polycaprolactone (PCL) is widely used in the field of tissue engineering,[1] biomaterials and packaging system for its excellent physicochemical properties of biocompatibility, biodegradability, processability, sharp memory function, low toxicity and drug permeability.[2–4]

PCL is commonly synthesized by the ring-opening polymerization (ROP) of ε-caprolactone (ε-CL) in bulk or organic solvents. On the one hand, the ROP mechanisms of ε-CL can be roughly divided into five categories, *i.e.*, anionic polymerization, cationic polymerization, organocatalytic polymerization, enzymatic polymerization, and coordination-insertion polymerization.[5] Among them, the coordination-insertion polymerization is well studied because it can produce PCL with a clear structure and controllable molecular weights.[6] On the other hand, there are a wide variety of systems used to catalyse the ROP of ε-CL. Currently, the most commonly used catalyst systems mainly contain four types, *i.e.*, metal-based compounds, enzymatic compounds, organic compounds and inorganic acids.[7]

Although PCL has remarkable properties as mentioned above, there are still some problems. The ROP of ε-CL is traditionally carried out by conventional heating, generally taking more than 24 h to complete.[8] It has high energy costs and is inefficient. Besides, similar to most biopolymers, the thermal properties and mechanical properties of PCL are not excellent enough, which limit the applications of PCL in high-temperature processing or high-strength devices. Even if PCL has potential in the field of solid polymer electrolytes (SPEs) of lithium-ion batteries,[9–11] it is semi-crystalline, which obstructs the transport of lithium ions in PCL-based SPE and leads to low ion conductivity.[12] Therefore, the use of energy efficient ε-CL polymerization crafts and improvements in the comprehensive performance of PCL are of important value.

Microwave-assisted heating is totally different from conventional heating. Microwave irradiation has been proved to dramatically accelerate the polymerization of monomers, which contain polar groups that absorb microwaves.[13] Over the last decades, microwave irradiation has developed into a highly useful technique and an effective alternative energy source for chemical reactions and processes.[14] Compared with conventional heating ring-opening polymerization (HROP), microwave-assisted ring-opening polymerization (MROP) has

Faculty of Materials Science and Chemistry, China University of Geosciences, Wuhan 430074, China. E-mail: ruima@cug.edu.cn; jinhongyun@cug.edu.cn

† Electronic supplementary information (ESI) available. See DOI: 10.1039/d1ra07469e

many advantages, including rate enhancement, environmentally friendly, safety, high-temperature homogeneity and manufacture of high-value low-volume chemicals.[15] Thus, MROP is an environmental and high-efficiency technique for the synthesis of PCL.

In recent years, polymer matrix composites have been greatly developed by the integration of organic and inorganic fillers into polymers.[16] Their various properties, such as ion conductivity, mechanical properties and thermal stability,[17–19] have improved significantly compared with pure polymers. In this way, high-performance PCL matrix composites can be produced. Halloysite is a kind of natural layered silicate mineral, containing rich silicon and aluminate active sites. It is chemically similar to kaolinite and have a chemical formula of $Al_2(OH)_4Si_2O_5 \cdot (0–2)H_2O$.[20] Halloysite nanotubes (HNTs) are the dominant form of natural halloysite, with a multi-layered tubular structure.[21] The global supply of HNTs exceeds thousands of tons per year and HNTs are low-cost, meaning that mass-scale industrial applications can be achieved.[22] HNTs are a kind of promising filler for high-performance polymer matrix composites,[23] due to their high specific surface area (SSA), high aspect ratio, good dispersion, nontoxicity, high strength, and excellent thermal stability.[24] Furthermore, HNTs are widely used in the catalysis industry, as additives in catalytic systems or promising materials for the preparation of heterogeneous catalysts, *etc.*25–29 As far as HNTs are concerned, the abundant hydroxyl groups on the internal lumen surface and aluminate active sites have the synergetic catalytic ability in the case of ROP of ε-CL.[30] However, if only catalyzed by HNTs, the chain growth of the polymerization results in short chains, which is manifested by the low molecular weight and poor performance of corresponding PCL products. A better option is to use HNTs as the support of catalysts. Due to the tubular structure, high SSA and active sites, HNTs are of great application value as a host for the loading of various guests.[31–33] By loading certain catalysts on modified HNTs through physical forces or chemical reactions, a composite catalytic system with excellent catalytic performance can be constructed. In the polymerization catalyzed by the composite catalytic system, the chain growth starts at the active sites on the surface of HNTs, and *in situ* polymerization occurs. Compared with physically blending fillers with polymers, fillers can be better dispersed in the polymer matrix by *in situ* polymerization, and the interactions are stronger among the polymer, surfactant and filler surface.[34] Correspondingly, PCL-HNTs synthesized by the composite catalytic system have better performance and higher molecular weight than the PCL matrix nanocomposites catalyzed by only HNTs or physically blending with inorganic fillers.

In this work, a composite catalytic system, modified halloysite nanotubes loaded with stannous chloride (APTES-P-h-HNTs-$SnCl_2$), was creatively synthesized. It not only has excellent catalytic ability but also acts as the performance-enhancing filler of polymer matrix composites. The microwave-assisted *in situ* ROP of ε-CL in the presence of APTES-P-h-HNTs-$SnCl_2$ was carried out to synthesize PCL-HNTs and their structures, thermal properties and electrochemical performances were significantly investigated.

2. Experimental

2.1. Materials

ε-Caprolactone (ε-CL, 99%), from Alladin, was distilled under vacuum and stored with a calcined molecular sieve. High-purity halloysite nanotubes (HNTs), from Yuanxin Nano Technology Co., Ltd (Guangzhou, China), were vacuum dried before use. Stannous chloride ($SnCl_2$, 99%), from Mucklin, was used without further purification. (3-Aminopropyl)triethoxysilane (APTES, $H_2NCH_2CH_2CH_2Si(OC_2H_5)_3$, ≥98%), from Lvwei New Material Technology Co., Ltd (Guangdong, China), was used without further purification. All other reagents were used as received.

2.2. Preparation of APTES-P-h-HNTs-$SnCl_2$

As shown in Scheme 1, 4.00 g of HNTs were dispersed in 200 mL deionized water. Subsequently, 0.116 g NaOH was added and the mixture was magnetically stirred for 24 h at room temperature.[35] The solid phase of the resultant hydroxylated HNTs (h-HNTs) was obtained by centrifugal separation and rinsed several times with water until the pH of the filtrate reached 7. The prepared h-HNTs were first dried at 60 °C for 2 h in an oven and then dried at 60 °C in a vacuum oven for 24 h.

The h-HNTs obtained were calcined at 400 °C for 3 h to remove the interlayer water of HNTs.[36] Then, calcined h-HNTs were ground into powder using a quartz mortar. To physically load $SnCl_2$ onto the surface of h-HNTs, $SnCl_2$ (2.10 mmol), toluene (45 mL) and h-HNTs (3.33 g) were added to a 150 mL reaction flask with a branch nozzle. The APTES (2.55 mmol) and toluene (25 mL) were also added to a 50 mL beaker and well mixed.[37] The ligand solution in the beaker was then added to the reaction flask and three nitrogen purge cycles were applied to the reaction flask. Finally, the solution system was stirred overnight to obtain the composite catalytic system of APTES-P-h-HNTs-$SnCl_2$.

2.3. Microwave-assisted *in situ* ROP

Microwave-assisted polymerizations were carried out in an MCR-3 atmospheric-pressure microwave chemical reactor. The typical procedure was as follows. A mixture of ε-CL and corresponding certain proportions of APTES-P-h-HNTs-$SnCl_2$ or $SnCl_2$ (as the control groups) were ultrasonically mixed and then placed into a three-necked reaction flask. Through three times of vacuum–nitrogen cycles, the mixture was irradiated and then polymerized at certain constant temperatures stabilized by the reaction microwave power of 400 W. The crude solid product was dissolved in methylene chloride and precipitated using methanol. The precipitate was filtered and dried under a vacuum at 40 °C.

In the following content, PCL-HNTs and PCL, respectively, represented products from ε-CL catalyzed by APTES-P-h-HNTs-$SnCl_2$ and $SnCl_2$. Moreover, PCL-HNTs (1 wt%) and PCL-HNTs (3 wt%), respectively, represented PCL-HNTs [initiator/monomer (I/M) mass ratio = 1%] and PCL-HNTs (I/M mass ratio = 3%).

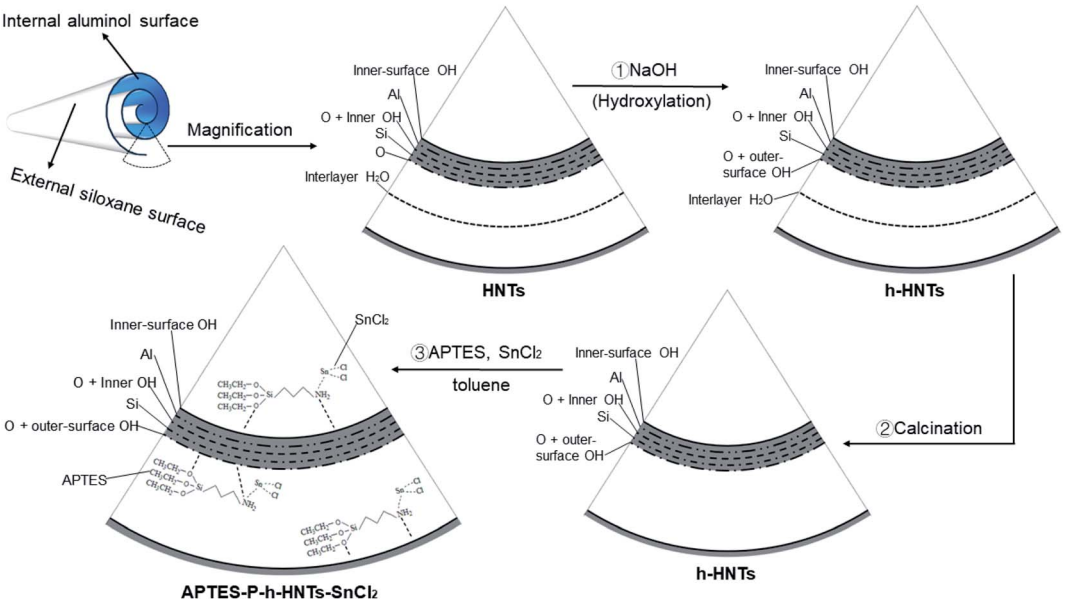

Scheme 1 Schematic illustration of structures and preparation processes from HNTs to APTES-P-h-HNTs-$SnCl_2$.

2.4. Fabrication of composite polymer electrolytes

Composite polymer electrolytes (CPEs) were prepared by a solution casting method.[38] Appropriate amounts of PCL-HNTs and LITFSI to give [O] : [Li] ratio of 20 : 1 were dissolved in dimethyl carbonate, and the solution was stirred at 55 °C for 2 h. A predetermined amount of Al_2O_3 powder with different particle size was then added, and the solution was mixed for 24 h with continuous heating. When complete homogenization of a mixture occurred, the solution was cast on a glass plate using a doctor blade. Residual solvent was completely removed by drying the electrolyte film at room temperature for another 24 h. Then, the obtained CPEs membranes were cut into circular rounds with a diameter of 19 mm and placed in an Ar-filled glove box overnight to remove the residual solvent and finally for electrochemical tests.

2.5. Measurements

X-ray photoelectron spectroscopy (XPS) was performed on a 'Thermo Scientific K-Alpha' with an Al Kα source (1486.6 eV). The full-spectrum scan (pass energy: 160 eV) and the narrow-spectrum scan (pass energy: 50 eV) were conducted on all samples. All spectra were calibrated using the C 1s peak (284.80 eV).

^{1}H NMR spectra were recorded on a 'Bruker 400M' spectrometer using tetramethylsilane as an internal standard and $CDCl_3$ as a solvent.

X-ray diffraction (XRD) patterns were performed on a 'Bruker D8 Advance' with Cu Kα radiation, in the 2θ rotation range of −110° to 168°.

Hitachi SU8010 high-resolution field emission scanning electron microscope (SEM) was applied to investigate the surface morphology and cross-sectional structure of HNTs, APTES-P-h-HNTs-$SnCl_2$, PCL and PCL-HNTs.

The number-average molecular weight (M_n) and polymer dispersity index (PDI) of PCL-HNTs were determined using gel permeation chromatography (GPC) of a 'Breeze 2 Hplc 1525' instrument. *N*,*N*-Dimethylformamide was used as an eluent at a flow rate of 1.0 mL min^{-1} and GPC data were calibrated by standard polymethyl methacrylate.

Differential scanning calorimetry (DSC) was performed using a 'Netzsch DSC 204 F1' and the test process was set as followed. Firstly, at a heating rate of 20 °C min^{-1}, samples were heated from ambient temperature to 80 °C, and kept isothermally at 80 °C for 10 minutes. Secondly, at a temperature ramp rate of 50 °C min^{-1}, samples were cooled from 80 °C to −80 °C, and maintained under isothermal temperature for 10 minutes. Finally, samples were heated from −80 °C to 80 °C at a heating rate of 20 °C min^{-1}.

Thermal stabilities were performed using a 'Netzsch STA 2500'. The sample was heated from 30 °C to 630 °C in a nitrogen atmosphere at a heating rate of 10 °C min^{-1}, without heat preservation.

AC impedance and ionic conductivity measurements on CPEs were performed using a 'Zennium X' Zahner electrochemical workstation over the frequency range of 10 MHz to 100 mHz. CPE films were sandwiched between two stainless steel disk electrodes and measured from 30 °C to 60 °C. The charge/discharge tests were performed using a 'CT2001A' from the LAND system.

3. Results and discussion

3.1. Effect of modification treatments on HNTs

XPS survey scans of HNTs and APTES-P-h-HNTs-$SnCl_2$ are shown in Fig. 1. Characteristic elements including aluminium, carbon, chlorine, sodium, oxygen, silicon and tin were detected.

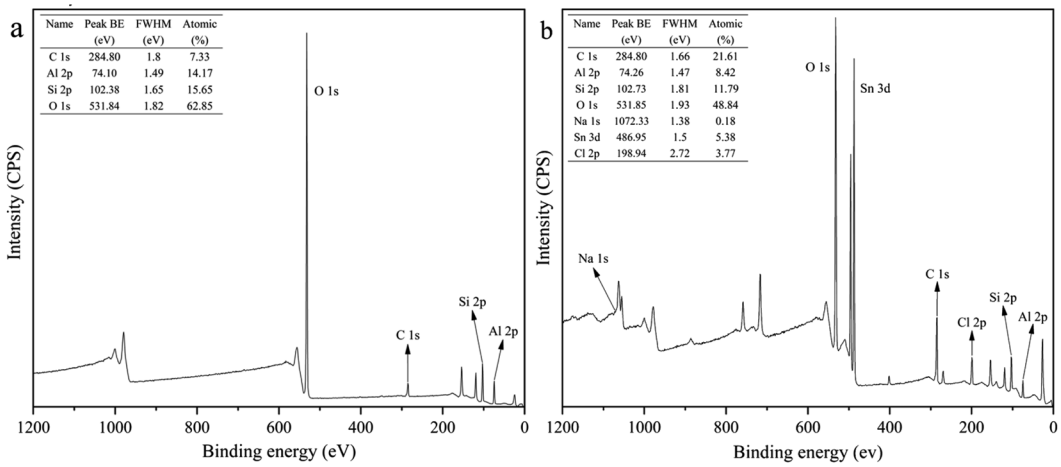

Fig. 1 XPS survey scans of (a) HNTs, (b) APTES-P-h-HNTs-$SnCl_2$.

Sodium was only detected in APTES-P-h-HNTs-$SnCl_2$, confirming the effectiveness of the hydroxylation treatment. The relative concentrations of aluminium to oxygen and silicon to oxygen both decreased from HNTs to APTES-P-h-HNTs-$SnCl_2$. This can be ascribed to the alkaline etching of aluminium oxide octahedral layers and silicon oxide tetrahedron layers of HNTs. Since the inner and outer surfaces of HNTs were reactive during the hydroxylation treatment, parts of aluminium and silicon were dissolved in the form of AlO_2^- and SiO_3^{2-} (aq.), and extra aluminium hydroxyl groups and silanol groups were generated.

Tin and chlorine were only detected in APTES-P-h-HNTs-$SnCl_2$, confirming the effectiveness of the silane coupling agent treatment and physical loading of stannous chloride. The atomic percentages of tin and chlorine were 5.38% and 3.77%. This is because the HNTs were physically absorbed with APTES acting simultaneously as a support and a ligand of stannous chloride. The stannous chloride catalyst was physically adsorbed onto the surface of HNTs.

Fig. 2(a) exhibited the microscopic morphology of HNTs, including high aspect ratios, smooth surfaces and tubular structures. This also reflected the high purity of HNTs used in this work. Otherwise, the morphology of APTES-P-h-HNTs-$SnCl_2$ could be seen in Fig. 2(b), showing a clear difference from HNTs. After hydroxylation, calcination, silane coupling agent modification and stannous chloride physical adsorption, the halloysite nanotubes still had a high aspect ratio, but the tubular structure was damaged and there were obvious particles on the surface with attachments. SEM micrographs more intuitively proved the success of the above modifications of HNTs.

3.2. PCL-HNTs characterization

Hard and lumpy products were obtained when ε-CL was irradiated using microwaves in the presence of APTES-P-h-HNTs-$SnCl_2$. As shown in Table 1, the M_n values of the products ranged from 9700 to 53 000 g mol^{-1} with a polymer dispersity index (M_w/M_n) of 1.11–1.61.

The influence factors of polymerization, including polymerization temperatures stabilized by MCR-3 with certain microwave power, I/M mass ratios and the time of microwave irradiation, were investigated. In this work, the reaction microwave power was 400 W, polymerization temperatures were set to 210 °C and 250 °C, initiator/monomer (I/M) mass ratios were respectively 1% and 3%, and the irradiation time was from 5 to 60 min. Among them, the best conditions for the microwave-assisted *in situ* ROP of ε-CL were obtained, carrying out polymerizations at 250 °C, when the I/M mass ratio is 1%.

^{1}H NMR analyses revealed the expected structures of the synthesized products under the experimental conditions. ^{1}H

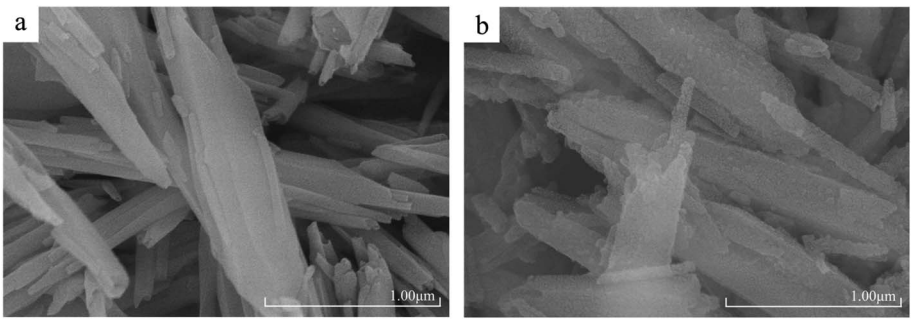

Fig. 2 SEM micrographs of (a) HNTs, (b) APTES-P-h-HNTs-$SnCl_2$.

Table 1 Microwave-assisted *in situ* ROP of ε-CL

n	I/M (wt%)	*T* (°C)	*t* (min)	CR (%)	M_n (g mol^{-1})	PDI
1	1	210	30	80.1	19 497	1.29
2	1	210	40	81.4	20 426	1.56
3	1	210	60	82.5	21 997	1.39
4	1	250	5	36.3	14 134	1.11
5	1	250	10	79.3	23 913	1.40
6	1	250	20	88.8	29 711	1.56
7	1	250	30	93.2	36 482	1.56
8	1	250	40	94.8	48 161	1.52
9	1	250	60	93.9	52 088	1.48
10	3	250	5	25.2	9785	1.11
11	3	250	10	71.0	21 253	1.12
12	3	250	20	86.9	24 472	1.61
13	3	250	30	93.9	30 031	1.57
14	3	250	40	92.3	31 777	1.51
15	3	250	60	94.8	32 494	1.52

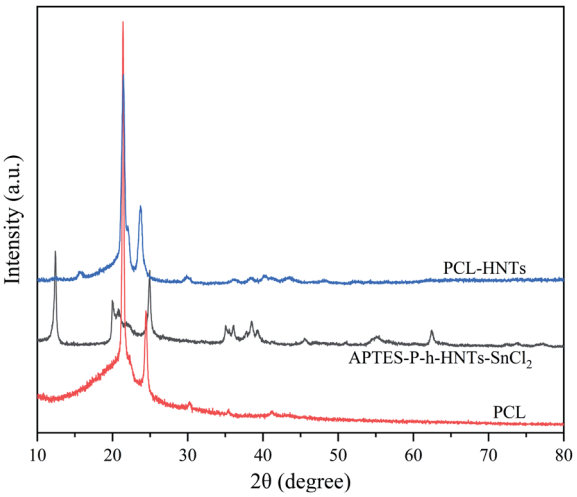

Fig. 4 XRD patterns of PCL, APTES-P-h-HNTs-$SnCl_2$ and PCL-HNTs.

NMR (400 MHz, chloroform-d, δ): 7.26 (s, 2H; Ar H), 4.05 (t, J = 6.7 Hz, 2H; OCH_2), 2.29 (t, J = 7.5 Hz, 2H; CH_2CO), 1.82–1.50 (m, 4H; CH_2), 1.38 (d, J = 7.2 Hz, 2H; CH_2) (Fig. 3). The ^{1}H NMR spectrum of the synthesized products was the same as the authoritative sample of PCL.[39]

APTES-P-h-HNTs-$SnCl_2$, PCL and PCL-HNTs were characterized using XRD, as shown in Fig. 4. The XRD pattern of PCL-HNTs was compared with those of PCL and HNTs to identify the characteristic peaks. PCL and HNTs exhibited characteristic peaks, showing semi-crystalline and crystalline nature, respectively.[40] The appearance of all peaks in PCL-HNTs confirmed the presence of the two constituents.

The above results indicated that PCL-HNTs were successfully synthesized when the ROP of ε-CL was irradiated using microwaves and APTES-P-h-HNTs-$SnCl_2$ as catalysts. As shown in Scheme 1 and Table 2, it could be inferred from the synthetic path of the composite catalytic system that there were three modes of the polymer molecular chain growth. In a first way, chain initiation occurred on the hydroxyl groups on the surface of the modified halloysite nanotubes, and the active hydrogen in the hydroxyl group attacked the C–O bond in caprolactone for the chain growth, resulting in PCL grafting on HNTs.[30,41] The acidic nature of HNTs was the source of the polymerization behaviour. The ROP mechanism was cationic polymerization. The second was that hydroxyl groups on the surface of the modified HNTs reacted with $SnCl_2$ to form alkoxy-tin, and then alkoxy-tin was coordinated with ε-CL to achieve the ROP of ε-CL, and the PCL grafted on HNTs was generated.[42] The mechanism of ROP was coordination-insertion polymerization. The third was that chain initiation occurred on the stannous chloride physically loaded on the surface of the modified halloysite. The tin in the stannous chloride was coordinated with ε-CL, carrying out ROP of ε-CL and generating free PCL. The ROP mechanism was coordination-insertion polymerization.

Among the three polymer chain growth modes, the last was the main one, because free PCL accounts for about three quarters in PCL-HNTs(1 wt%). The specific calculation method was to dissolve appropriate amounts of PCL-HNTs(1 wt%) in dichloromethane and centrifuge them at 10000 rpm. The solid component obtained by centrifugation was dissolved in dichloromethane and centrifuged at 10000 rpm again. The finally obtained solid component was APTES-P-h-HNTs-$SnCl_2$ and its proportion of the mass of the APTES-P-h-HNTs-$SnCl_2$ originally used corresponded to the proportion of the free PCL.

We reasoned that there existed a synergistic catalytic effect between the hydroxyl groups and the metal center, different from the catalytic action in simple metal-catalyzed reactions or organic catalytic reactions. All chain growth mechanisms

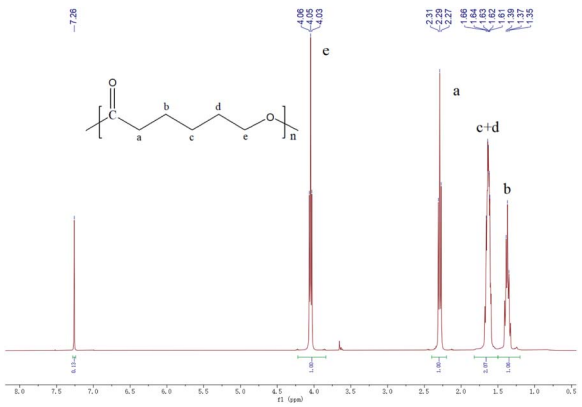

Fig. 3 ^{1}H NMR spectrum of PCL-HNTs.

Table 2 The grafting rate of PCL-HNT nanocomposites

Sample	Free PCL rate (%)	Grafting rate (%)
PCL-HNTs(1 wt%)-10 min	83.3	16.7
PCL-HNTs(1 wt%)-20 min	80.1	19.9
PCL-HNTs(1 wt%)-30 min	76.5	23.5
PCL-HNTs(1 wt%)-40 min	78.2	21.8
PCL-HNTs(1 wt%)-60 min	72.1	27.9

simultaneously proceeded between the layers or on the surface of HNTs, conducting *in situ* ROP of ε-CL.

PCL and PCL-HNTs were subjected to liquid nitrogen brittle cooling and fracture operations to prepare samples. A high-resolution field emission scanning electron microscope was used to observe the cross-section of the sample and SEM micrographs of the synthesized PCL, PCL-HNTs(1 wt%) are exhibited in Fig. 5. The SEM micrograph of PCL shown in Fig. 5(a) indicated an obvious layer-packed structure, with some small pits. The local longitudinal morphology of high magnification was shown in Fig. 5(b), which showed that the distribution directions of the slice layers were consistent.

Fig. 5(c) is the SEM micrograph of PCL-HNTs(1 wt%) and totally different morphologies from PCL were observed. Catalyzed by APTES-P-h-HNTs-$SnCl_2$, the microscopic morphology of PCL-HNTs(1 wt%) was no longer a lamellar structure, but a petal-like structure instead. Moreover, a porous structure appeared and distributed uniformly, and the average diameter of pits was slightly increased. The high-magnification local morphology of Fig. 5(d) clearly showed the petal-like structure of PCL-HNTs(1 wt%). The petals were even intertwined and interlaced, leaving many pores among them. The huge difference in the microscopic morphology of PCL-HNTs(1 wt%) and PCL could be explained by the fact that the chain initiation and chain growth of PCL-HNTs(1 wt%) were carried out on the active sites of the modified HNTs, macroscopically growing around HNTs due to the template effect. However, the polymerization for PCL was just a conventional chain proliferation catalyzed by $SnCl_2$.

Structural differences between PCL and PCL-HNTs were apparent in their respective properties. The layered structure of PCL meant that it was prone to deformation and fracture when it was stressed. The absence of a porous structure also led to a stress concentration. Overall, the mechanical properties of PCL were brittle and soft. However, for PCL-HNTs, the petal-shaped three-dimensional connection structure guaranteed their mechanical strength, and HNTs themselves were also excellent polymer-reinforcing fillers, which helped to improve the mechanical properties of polymer nanocomposites. Meanwhile, the porous structure could disperse stress and enhance the toughness of PCL-HNTs. Overall, the mechanical properties of PCL-HNTs were tough and hard. In this work, the film-forming properties of PCL and PCL-HNTs verified their respective mechanical properties, and the film-forming properties of the latter were far superior to the former.

3.3. Thermal properties

Thermal stabilities and thermal characterizations of PCL and PCL matrix nanocomposites with HNTs were respectively determined by thermogravimetry and differential scanning calorimetry.

For thermal stabilities of polymer/filler nanocomposites could be affected by the polymer matrix, the filler and the interaction between the polymer matrix and the filler.[43] In order to study these factors, targeted experiments were carried out, and the results were shown in Fig. 6. Sample b was the composite of PCL and HNTs prepared by physical blending.

As shown in Table 3, for the polymer matrix, the thermal performance of PCL was not excellent enough, the decomposition temperatures for the loss of 1 wt% and 5 wt% were 214.6 °C and 252.1 °C, respectively. For fillers, no matter how HNTs participate in the polymerization of ε-CL, the initial

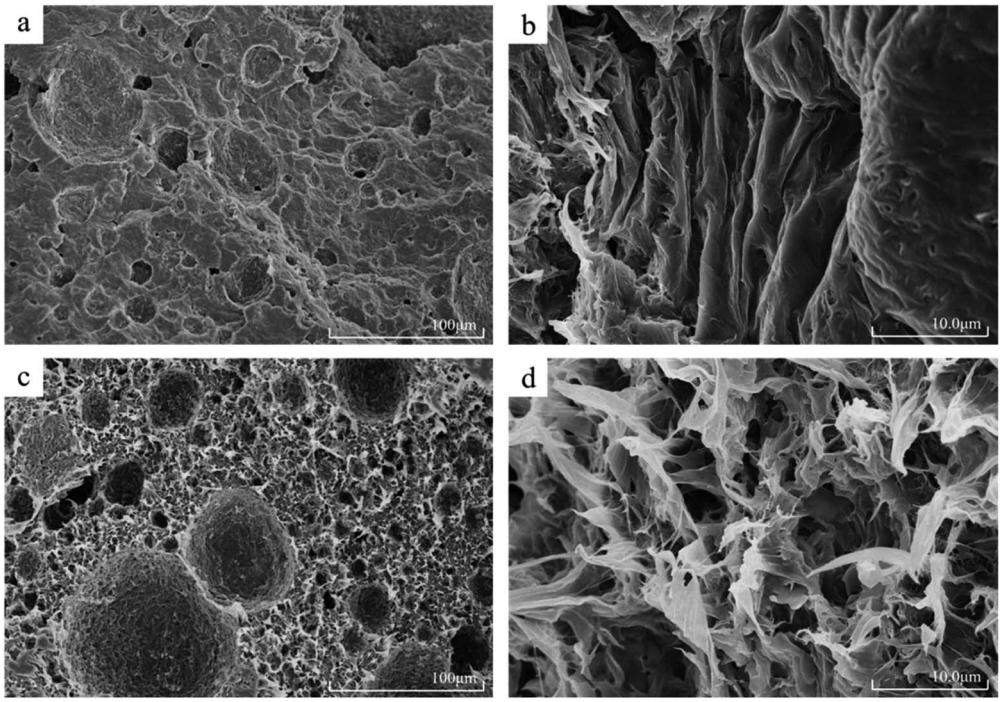

Fig. 5 SEM micrographs of PCL (a) and (b) and [PCL-HNTs(1 wt%)] (c) and (d).

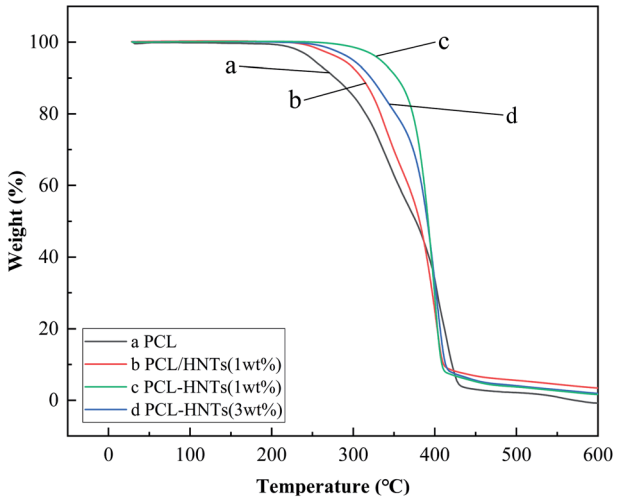

Fig. 6 Thermogravimetric analysis curves of PCL and PCL matrix nanocomposites with HNTs.

decomposition temperature of PCL matrix nanocomposites with HNTs was 31.4–81.2 °C, higher than PCL. The dispersion of fillers into the polymer matrix could help improve thermal stabilities because fillers could act as a superior insulator and mass transport barrier to the volatile products generated during decomposition.[44] For the interaction between the polymer matrix and filler, the compatibility and dispersibility of the filler in the polymer matrix played a decisive role. For samples b and sample c, the mass ratios of HNTs to PCL were both 1%. In sample b, HNTs were physically mixed into the PCL matrix. However, in sample c, HNTs were first modified by APTES to increase their compatibility with polymers and then participated in the *in situ* ROP of ε-CL as the carrier and ligand of the composite catalytic system, which further improved the compatibility and dispersibility of HNTs in the PCL matrix. Therefore, comparing the above two samples, the initial decomposition temperature of sample c was about 45 °C higher than that of sample b.

As proved from the thermal stability of four representative samples, APTES-P-h-HNTs-$SnCl_2$ had good dispersibility and compatibility in the PCL matrix, and thermal stabilities of PCL-HNTs had been significantly improved, compared to that of PCL.

For thermal characterization of PCL and PCL matrix nanocomposites with HNTs, DSC thermograms of samples in the re-melting process were measured and are shown in Fig. 7. The melting temperature (T_m), the heat of fusion (ΔH_m) and associated degree of crystallinity (χ_c) obtained from DSC measurements are summarized in Table 4. χ_c was calculated using the heat of fusion per gram of samples determined from the DSC measurements and heat of fusion corresponding to 100% crystalline PCL (136 J g^{-1}).[45] It is shown in Table 4 that the values of χ_c were reduced in the case of PCL matrix nanocomposites with HNTs as compared to PCL. This was due to the decrease in molecular mobility of PCL chains in nanocomposites that caused a reduction in the PCL crystal size and imperfections of the crystals.[46] Similar behaviours were also observed for PCL/clay nanocomposites.[47] In general, the crystallinity and melting point of the same material were positively correlated. Although the crystallinity of PCL matrix nanocomposites with HNTs was lower than the crystallinity of PCL, the melting point was maintained or even increased. This was because in PCL matrix nanocomposites with HNTs, intermolecular hydrogen bonds were formed between molecular chains and hydroxyls on the surface of modified HNTs and silane coupling agents.

3.4. Electrochemical performance of CPEs

The polymer matrix of CPEs(PCL-HNTs) contained PCL-HNTs(1 wt%). The ionic conductivity (σ) values of electrolyte CPEs were determined using electrochemical impedance spectroscopy (EIS). Fig. 8(a) shows the Nyquist plot of the CPEs(PCL-HNTs) membrane. The semicircle at high frequency

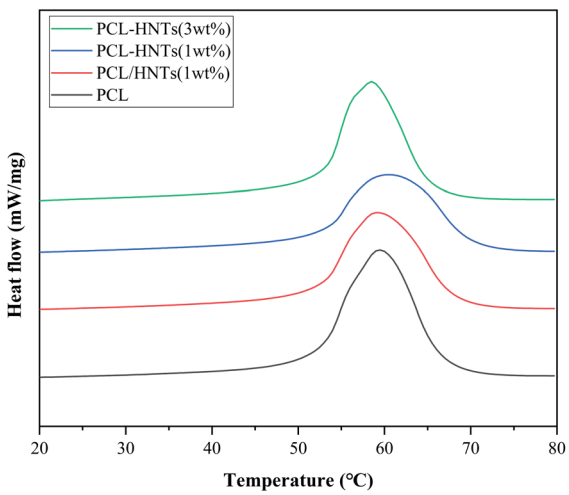

Fig. 7 DSC thermograms of PCL and PCL matrix nanocomposites with HNTs during the reheating process.

Table 3 Decomposition temperatures of PCL and PCL matrix nanocomposites with HNTs

Sample	T_d (1 wt% loss)	T_d (5 wt% loss)
a – PCL	214.6 °C	252.1 °C
b – PCL/HNTs(1 wt%)	246.0 °C	287.5 °C
c – PCL-HNTs(1 wt%)	291.6 °C	333.3 °C
d – PCL-HNTs(3wt%)	259.7 °C	299.7 °C

Table 4 Thermal characteristics of PCL and PCL matrix nanocomposites with HNTs

Sample	T_m (°C)	ΔH_m (J g^{-1})	χ_c (%)
PCL	52.4	58.42	43.0
PCL/HNTs(1 wt%)	52.4	48.82	35.9
PCL-HNTs(1 wt%)	53.0	42.54	31.3
PCL-HNTs(3 wt%)	52.9	47.08	34.6

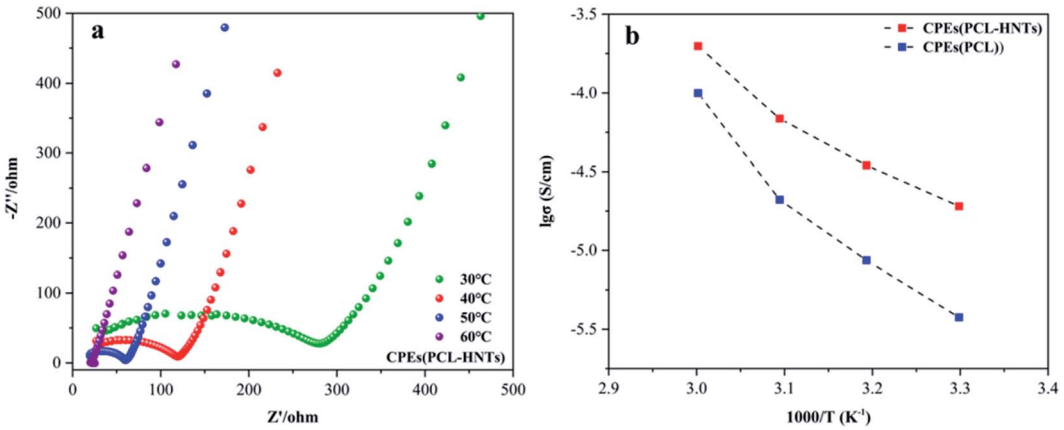

Fig. 8 (a) Nyquist of CPEs(PCL-HNTs), (b) the Li-ion conductivity of CPEs(PCL-HNTs) and CPEs(PCL).

represented the impedance belonging to the electrolyte body. The σ of CPEs(PCL-HNTs) electrolyte was 1.91×10^{-5} S cm^{-1} at 30 °C, which was more than five times as much as that of the CPEs(PCL) electrolyte (3.77×10^{-6} S cm^{-1}). The σ value increased with rising temperature, as shown in Fig. 8(b) and Table 5. Clearly, the σ of CPEs(PCL-HNTs) was always higher than that of CPEs(PCL) within the considered temperature range and finally reached up to 1.98×10^{-4} S cm^{-1} at 60 °C. This resulted from the lower χ_c of PCL-HNTs compared with PCL. During the transport of lithium ions in SPE, they coordinated with polar groups on the polymer chain at a specific position. Through the movement of the chain segment of polymer molecules, free volume appeared, so that lithium ions could be conducted within and between polymer molecular chains. In the polymer matrix, lower χ_c meant a greater proportion of amorphous regions, in which the segments could move at an ambient temperature higher than T_g. Therefore, lower χ_c of the polymer matrix caused higher σ of SPE.

CPEs(PCL) were too brittle to be used in tests of lithium metal solid-state batteries. To evaluate the performance of the prepared CPEs(PCL-HNTs) in lithium metal solid-state batteries, LFP//CPE//Li batteries were assembled, and the discharge capacity was monitored at 60 °C. As shown in Fig. 9(a) and (b), the discharge capacity displays a rising trend with the increase in the cycle number, indicating a slowly activating process of the cell. Then, the reversible discharge capacity remained at the level of 163 mA h g^{-1} during the 20th to 50th cycles, showing good discharge capacity and electrochemical stability of CPEs(PCL-HNTs).

Table 5 Conductivity of CPEs at different temperatures

Sample (S cm^{-1})	30 °C	40 °C	50 °C	60 °C
CPEs(PCL)	3.77×10^{-6}	8.65×10^{-6}	2.10×10^{-5}	9.98×10^{-5}
CPEs(PCL-HNTs)	1.91×10^{-5}	3.47×10^{-5}	6.88×10^{-5}	1.98×10^{-4}

4. Conclusion

The composite catalytic system of APTES-P-h-HNTs-$SnCl_2$ was prepared through hydroxylation, calcination, silane coupling agent modification and physical loading, and used as a catalyst for the microwave-assisted *in situ* ROP of ε-CL. Target products of PCL-HNTs were successfully synthesized and suitable polymerization conditions are microwave power of 400 W, I/M mass

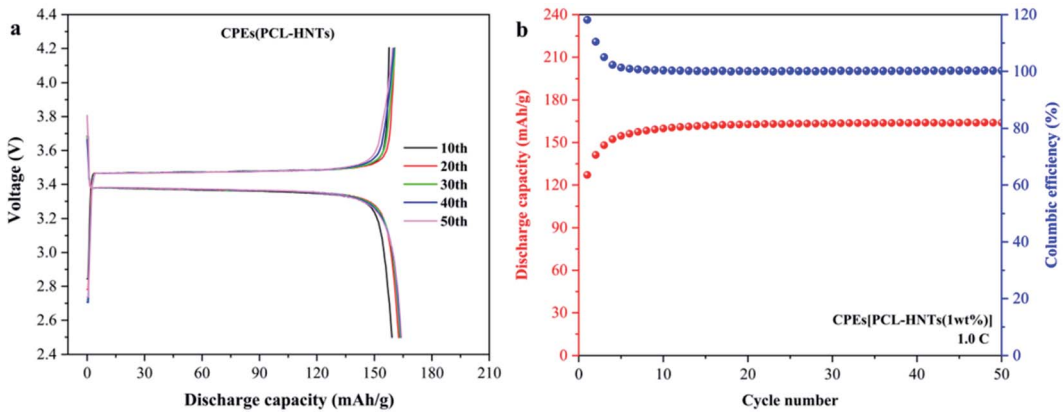

Fig. 9 (a) Charge and discharge profiles, (b) cycle performance of CPEs(PCL-HNTs) in $LiFePO_4$/CPEs/Li-battery.

ratio of 1% and polymerization temperature of 250 °C. Compared with PCL, PCL-HNTs are observed to have connected petal-like and porous structures for the template effect of the catalyst and have much better film-forming and thermal stabilities. Moreover, lower χ_c of PCL-HNTs causes SPE made by PCL-HNTs to have higher lithium-ion conductivity. Meantime, CPEs(PCL-HNTs) have good discharge capacity and electrochemical stability, showing the application potentiality of PCL-HNTs in SPE. So, APTES-P-h-HNTs-$SnCl_2$ is believed to not only act as a kind of an effective and efficient catalyst for the ROP of ε-CL but also effectively improve multiple properties of the PCL matrix, producing high-performance PCL-HNTs.

Author contributions

Rui Ma and Hongyun Jin conceived the project. Gang Yang conducted the synthesis of materials and characterizations. Shifan Zhang helped pre-process some materials. Ziying Liu and Dexuan Pei conducted the electrochemical tests. Wenjie Du and Jiaqi Liu helped analyze the data. Gang Yang wrote the paper, Rui Ma and Hongyun Jin helped polish this manuscript. All the authors discussed the results and commented on the manuscript.

Conflicts of interest

There are no conflicts to declare.

Acknowledgements

This work was supported by grants from the National Natural Science Foundation of China (51903080), Natural Science Foundation of Hubei Province (2018CFC854), Scientific Research Foundation of Hubei University of Science and Technology (2019-20KZ06), the Open Project of Key Laboratory of Green Chemical Engineering Process of Ministry of Education (GCP20200210).

References

1 R. M. Mohamed and K. Yusoh, *Adv. Mater. Res.*, 2016, **1134**, 249–255.
2 J. M. Williams, A. Adewunmi, R. M. Schek, C. L. Flanagan, P. H. Krebsbach, S. E. Feinberg, S. J. Hollister and S. Das, *Biomaterials*, 2005, **26**, 4817–4827.
3 F. Tay, D. Pashley, R. Loushine, S. Kuttler, F. Garcia-Godoy, N. King and M. Ferrari, *American Journal of Dentistry*, 2007, **20**, 365.
4 Q. Meng, J. Hu, Z. Yong, L. Jing and L. Yan, *J. Appl. Polym. Sci.*, 2007, **106**, 2515–2523.
5 P. Lecomte and C. Jérôme, *Synthetic biodegradable polymers*, 2011, pp. 173–217.
6 P. Lecomte and R. Jérme, Ring Opening Polymerization, in *Encyclopedia of Polymer Science and Technology*, 2004.
7 M. Labet and W. Thielemans, *Chem. Soc. Rev.*, 2009, **38**, 3484–3504.
8 X. M. Deng, M. L. Yuan, C. D. Xiong and X. H. Li, *J. Appl. Polym. Sci.*, 2015, **71**, 1941–1948.
9 D. Zhang, L. Zhang, K. Yang, H. Wang, C. Yu, D. Xu, B. Xu and L.-M. Wang, *ACS Appl. Mater. Interfaces*, 2017, **9**, 36886–36896.
10 T. Eriksson, J. Mindemark, M. Yue and D. Brandell, *Electrochim. Acta*, 2019, **300**, 489–496.
11 Y. Seo, Y.-C. Jung, M.-S. Park and D.-W. Kim, *J. Membr. Sci.*, 2020, **603**, 117995.
12 Q. Zhou, J. Ma, S. Dong, X. Li and G. Cui, *Adv. Mater.*, 2019, **31**, 1902029.
13 D. M. Mingos and D. R. Baghurst, *ChemInform*, 2010, **22**, 301.
14 D. Adam, *Nature*, 2003, **421**, 571–572.
15 C. R. Strauss, *Microwaves in organic synthesis*, 2002, pp. 35–60.
16 S. Ramakrishna, J. Mayer, E. Wintermantel and K. W. Leong, *Compos. Sci. Technol.*, 2001, **61**, 1189–1224.
17 E. Quartarone, P. Mustarelli and A. Magistris, *Solid State Ionics*, 1998, **110**, 1–14.
18 Y. Xiang, Z. Peng and D. Chen, *Eur. Polym. J.*, 2006, **42**, 2125–2132.
19 Y. Tomita, T. Nakamura and A. Tago, *Opt. Lett.*, 2008, **33**, 1750–1752.
20 S. Balbir and I. D. R. Mackinnon, *Clays Clay Miner.*, 1996, **44**, 825–834.
21 P. Yuan, P. D. Southon, Z. Liu, M. Green and J. Antill, *J. Phys. Chem. C*, 2008, **112**, 15742–15751.
22 Y. M. Lvov, D. G. Shchukin, H. Mohwald and R. R. Price, *ACS Nano*, 2008, **2**, 814–820.
23 M. Liu, Z. Jia, D. Jia and C. Zhou, *Prog. Polym. Sci.*, 2014, **39**, 1498–1525.
24 P. Yuan, D. Tan and F. Annabi-Bergaya, *Appl. Clay Sci.*, 2015, **112–113**, 75–93.
25 K. Ariga, H. Abe, Q. Ji and Y. M. Lvov, in *Functional polymer composites with nanoclays*, 2016, pp. 207–222.
26 J. Ouyang, Z. Zhao, H. Yang, Y. Zhang and A. Tang, *Appl. Clay Sci.*, 2018, **152**, 221–229.
27 S. Sadjadi, *Appl. Clay Sci.*, 2020, **189**, 105537.
28 Z. Li, L. Liu, A. J. González and D.-Y. Wang, *Polym. Chem.*, 2017, **8**, 3926–3936.
29 P. Kumar, P. Gupta and C. Sharma, *Catal. Sci. Technol.*, 2021, **11**, 3775–3786.
30 R. Ma, P. Hu, J. Fan, W. Tang, T. Chen and L. Shi, *Polym.-Plast. Technol. Eng.*, 2018, 1–13.
31 B. P. G. R. R. Price and Y. Lvov, *J. Microencapsulation*, 2001, **18**, 713–722.
32 E. Abdullayev and Y. Lvov, *J. Nanosci. Nanotechnol.*, 2011, **11**, 10007–10026.
33 E. Abdullayev, K. Sakakibara, K. Okamoto, W. Wei, K. Ariga and Y. Lvov, *ACS Appl. Mater. Interfaces*, 2011, **3**, 4040–4046.
34 C. Zeng and L. J. Lee, *Macromolecules*, 2001, **34**, 4098–4103.
35 S. Zeng, C. Reyes, J. Liu, P. A. Rodgers and L. Sun, *Polymer*, 2014, **55**, 6519–6528.
36 G. Brindley and J. Goodyear, *Mineral. Mag. J. Mineral. Soc.*, 1948, **28**, 407–422.

37 S. Barrientos-Ramírez, G. M. de Oca-Ramirez, E. Ramos-Fernández, A. Sepúlveda-Escribano, M. Pastor-Blas and A. González-Montiel, *Appl. Catal., A*, 2011, **406**, 22–33.
38 X. Li, D. Wang, H. Wang, H. Yan, Z. Gong and Y. Yang, *ACS Appl. Mater. Interfaces*, 2019, **11**, 22745–22753.
39 Q. Liao, L. J. Liu, C. Zhang and F. He, *J. Polym. Sci., Part A: Polym. Chem.*, 2002, **40**, 1749–1755.
40 M. Chozhanathmisra, K. Pandian, D. Govindaraj, P. Karthikeyan, L. Mitu and R. Rajavel, *J. Chem.*, 2019, **2019**, 1–12.
41 G. Wang, R. Ma, T. Chen, C. Yan, J. Gao and F. Bao, *Polym.-Plast. Technol. Eng.*, 2013, **52**, 1193–1199.
42 M. Lahcini, S. Elhakioui, D. Szopinski, B. Neuer, A. El Kadib, F. Scheliga, M. Raihane, F. B. Calleja and G. Luinstra, *Eur. Polym. J.*, 2016, **81**, 1–11.
43 L. Liao, Z. Chao and S. Gong, *Die Unterrichtspraxis/Teaching German*, 2007, **28**, 1148–1154.
44 S. S. Ray and M. Bousmina, *Prog. Mater. Sci.*, 2005, **50**, 962–1079.
45 M. Avella, M. Errico, P. Laurienzo, E. Martuscelli, M. Raimo and R. Rimedio, *Polymer*, 2000, **41**, 3875–3881.
46 K. S. Lee and Y. W. Chang, *J. Appl. Polym. Sci.*, 2013, **128**, 2807–2816.
47 B. Lepoittevin, M. Devalckenaere, N. Pantoustier, M. Alexandre and P. Dubois, *Polymer*, 2002, **43**, 4017–4023.